



Energy Absorption Characteristics of a Novel Asymmetric and Rotatable Re-entrant Honeycomb Structure

Huifeng Xi¹ Jiachu Xu^{1*} Shende Cen¹ Shiqing Huang^{1*}

(¹MOE Key Laboratory of Disaster Forecast and Control in Engineering and School of Mechanics and Construction Engineering, Jinan University, Guangzhou 510632, China)

Received 23 October 2020; revision received 20 January 2021; Accepted 25 January 2021;
published online 6 March 2021

© The Chinese Society of Theoretical and Applied Mechanics 2021

ABSTRACT Based on the symmetric re-entrant honeycomb (S-RH) structure with negative Poisson's ratios, a novel asymmetric and rotatable re-entrant honeycomb (AR-RH) structure was proposed. Both the S-RH structure and AR-RH structure were produced by the 3D printing technology. Through experimental test and finite element simulation, the deformation mechanism and energy absorption characteristics of the AR-RH structure and the S-RH structure with negative Poisson's ratios at different impact velocities were compared. The experimental test and finite element simulation results show that the novel AR-RH structure with negative Poisson's ratios has stronger energy absorption capacity than the S-RH structure, and it has been verified that the rotatability of AR-RH can indeed absorb energy. Furthermore, the degree of asymmetry of the AR-RH structure was discussed.

KEY WORDS Asymmetric and rotatable re-entrant honeycomb structure, Dynamic compression, Energy absorption characteristics, Metal 3D printing technology

1. Introduction

The design of new lightweight materials and structures for energy-absorbing purposes is complex, requiring the structure to be able to withstand and mitigate blast loading while still being light in weight [1–5]. The symmetric re-entrant honeycomb (S-RH) structures, which exhibit the negative Poisson's ratio (NPR) effect, could offer a potential alternative solution to address these concurrent objectives.

When the structure has a negative Poisson's ratio, owing to its unique deformation behavior, it has better mechanical and physical properties (such as shear modulus, fracture toughness, impact strength and indentation resistance [6, 7]). A honeycomb structure with negative Poisson's ratio is an ideal choice for deformable wings [8–12] and other aerospace structures [13–15]. It has broad application prospects in biomedicine, aerospace and other fields of national defense science and technology [7]. Frost and Ashby [16] took the lead in discovering and proposing a negative Poisson's ratio effect on materials made up of honeycomb structures in 1982. It is an important finding that promoted the development and application of materials with negative Poisson's ratios. Researchers have been working on exploring the relationship between the internal geometry and mechanical properties of various structures with negative Poisson's ratios [2]. Choi and Lakes [17] and Zhang [18] analyzed the elastic behavior of concave-angle honeycomb structures with negative Poisson's ratios. Zied [19] enhanced the

* Corresponding authors. E-mails: txjch@jnu.edu.cn; thuangsq@jnu.edu.cn

in-plane stiffness and increased the “pull-up” capacity of the structure by changing the concave-angle honeycomb structure with negative Poisson’s ratio. Zhang [20] carried out the finite element simulation of the dynamic performance of honeycomb materials with negative Poisson’s ratios under in-plane impact load and discussed the influence of cell expansion angle and impact velocity on the in-plane impact deformation and energy absorption ability of honeycomb materials. Hou and Yin [21] used LS-DYNA to analyze the deformation modes of multi-concave-angle honeycomb and concave-angle honeycomb structures at different impact velocities and revealed the mechanism of how the unique negative Poisson’s ratios of concave-angle honeycomb structures improve their impact resistance. Lu [22] proposed a two-dimensional multi-cell-material mechanical model with negative Poisson’s ratio effect, composed of partial concave and partial regular hexagonal. The effect of the geometric size of the element cell on the shear modulus and stiffness of the material was studied. Shi [23] studied the performance characterization of honeycomb sandwich structure with negative Poisson’s ratio and optimized the structure design. Fan [24] studied the mechanical behavior and energy absorption characteristics of graded honeycomb structures under in-plane impact. Panda [25] studied the mechanical properties of 3D printed honeycomb structure through experiments and numerical simulations. Wang [26] summarized the recent research progress in mechanical properties and energy absorption characteristics of novel metal honeycomb structures.

The cell of S-RH structure is symmetric. In this study, a novel asymmetric and rotatable re-entrant honeycomb (AR-RH) structure with asymmetric cells is proposed. The AR-RH structure and normal S-RH structure are fabricated using the metal 3D printing technology, which can make a variety of complex structural models. The dynamic impact test and finite element simulation of the two models are carried out to compare the structural deformation modes, dynamic response and energy absorption characteristics of the two models under different impact velocities. The new AR-RH structure has better energy absorption and buffering capability against impact load than the traditional symmetric re-entrant honeycomb structure. It is expected to become a new kind of structure with negative Poisson’s ratio, having prospective applications in biomedicine, aerospace and other fields of national defense science and technology.

2. Asymmetric and Rotatable Re-entrant Honeycomb Cell and Structure Design

Compared with the S-RH structure, the novel AR-RH cell with negative Poisson’s ratio effect has different deformation mechanism. There are two main deformation mechanisms leading to the negative Poisson’s ratio effect of honeycomb materials: re-entrant mechanism and rotatable mechanism, and they are closely related to the excellent energy absorption. Modification on the basic and normal S-RH cell was introduced in this study. The purpose of this modification was to increase rotation of the structure to generate rotational kinetic energy absorption.

Two different structures were studied in the present work. The profiles of S-RH cell and AR-RH cell are shown in Fig. 1a, b. Here, S-RH has been studied for many years and was used as a baseline in this study. Figure 1a, b shows the normal symmetric and asymmetric rotatable unit cells. The design parameters of cells are as follows: h is the height of the cell model; l is the length of cell; m and n are the distances from the concave angle to the bottom and right side of the structure, respectively; and t is the thickness of the structure. In this study, the novel AR-RH cell will be developed through changing the location m_1 of the structural re-entrant angle (as shown in Fig. 1a). And the sizes of the two cells are:

$$\begin{aligned} \text{AR-RH cell: } & l_1 = 10 \text{ mm}, h_1 = 12 \text{ mm}, m_1 = \frac{h_1}{3}, n_1 = 3 \text{ mm}, t = 0.8 \text{ mm}; \\ \text{S-RH cell: } & l_2 = 10 \text{ mm}, h_2 = 12 \text{ mm}, m_2 = \frac{h_2}{2}, n_1 = 3 \text{ mm}, t = 0.8 \text{ mm} \end{aligned}$$

The novel AR-RH structure is developed by a combination of the AR-RH cell and its mirror cell to study the load bearing and deformation capacity. An AR-RH cell is attached to its mirror cell, with a horizontal strut that connects the concave angles of the two cells (as shown in Fig. 2a). Figure 2b shows the normal S-RH structure. The spaces between cells are the same for these two structures.

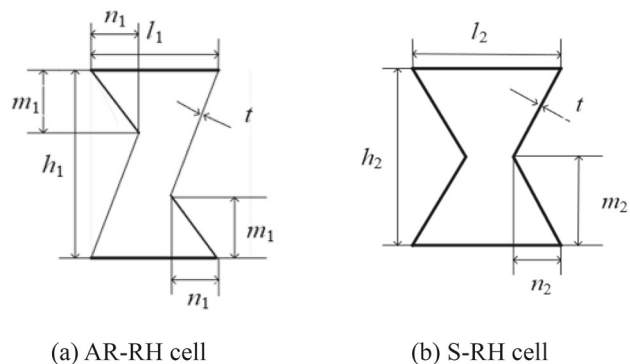


Fig. 1. Cell design: a asymmetric and rotatable re-entrant honeycomb (AR-RH) cell; b symmetric re-entrant honeycomb (S-RH) cell

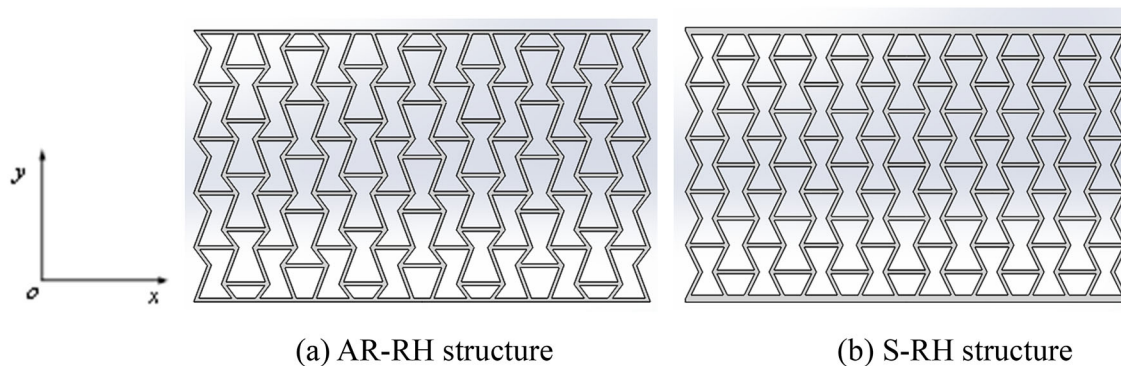


Fig. 2. Structure design: a asymmetric and rotatable re-entrant honeycomb (AR-RH) structure; b symmetric re-entrant honeycomb (S-RH) structure

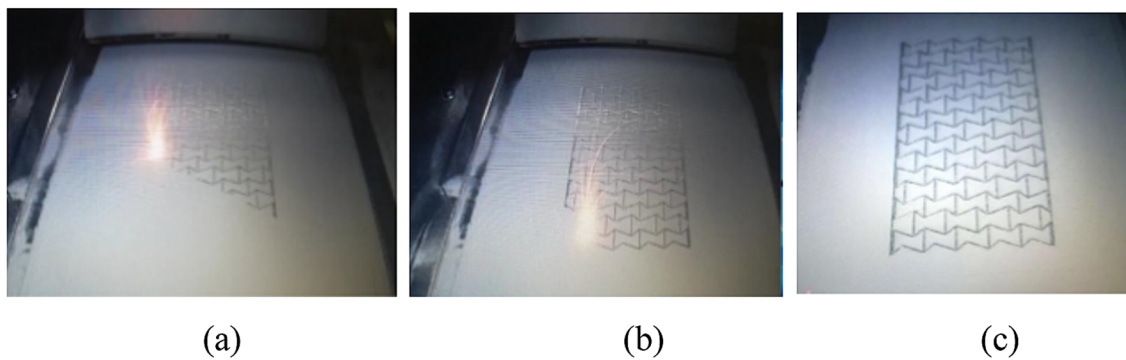
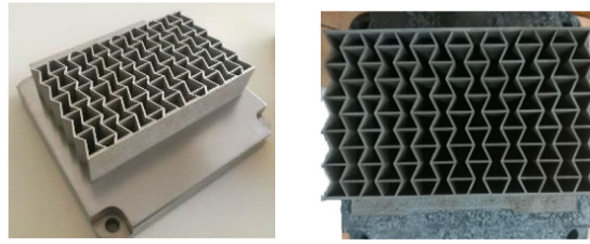


Fig. 3. 3D printing program: a \rightarrow b \rightarrow c

3. Sample Preparation Using 3D Printing Technology

The samples were manufactured using the 3D printing techniques (Farsoon Technologies, No. FS121M). The samples were made from 316L mineral powder, provided by Guangzhou Nalian Material Technology Co., LTD. Figure 3 shows the process of 3D printing layer by layer from bottom to top. Figure 4 displays the AR-RH structure and S-RH structure completed by 3D printing.

The mechanical properties of materials were determined from the tensile tests by ASTM D638-08 [27]. The dog-bone specimens were produced through 3D printing manufacturing process. The metal dog-bone specimens were tested by the hydraulic universal testing machine of MTS810 with digital image correlation technology. The material parameters are shown in Table 1.



(a) AR-RH structure (b) S-RH structure

Fig. 4. 3D printing model of AR-RH and S-RH structures

Table 1. Properties of 3D printing material

Density (kg/m^3)	Elastic modulus E (GPa)	Poisson's ratio μ	Yield stress (MPa)
7625.5	161.323	0.287	402

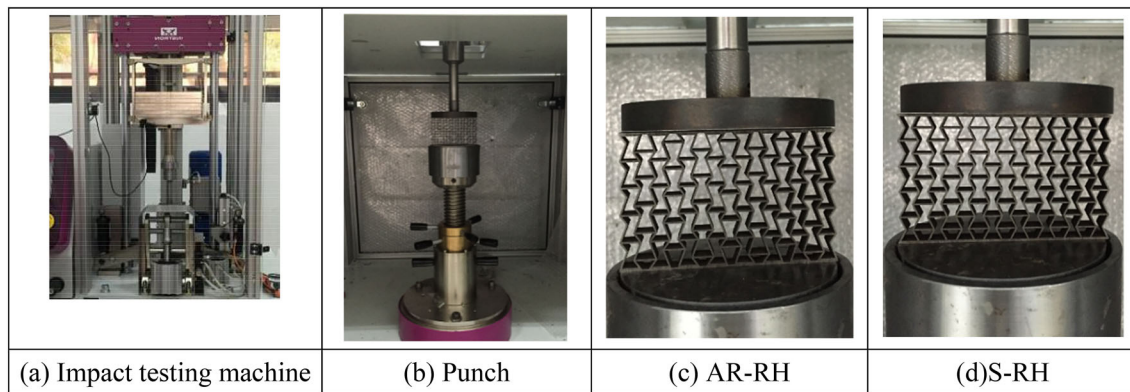


Fig. 5. Test setup and experimental model

4. Test and Simulation Design

4.1. Impact Test Design

Impact tests were conducted using the drop tower of CEAST 9350 Instron at different impact velocities. Three samples of both models were printed by 3D printing, with one specimen and divided equally into three groups. The impact velocities of three groups were 3 m/s, 4 m/s and 5 m/s, respectively. The added weight of the impact testing machine was 54.529 kg (including punch mass). The impact force, energy, displacement and speed of the impact process were collected. Through the impact experiments, the corresponding nominal stress–strain curves and energy–strain curves were obtained. The test device and experimental model are shown in Fig. 5.

4.2. Finite Element Simulation

Full-scale finite element models were constructed using ANSYS/LS-DYNA. The model was developed with shell element 163 and the full integration Belytschko–Tsay shell element algorithm to increase convergence. The AR-RH and S-RH structure models were placed between two rigid plates' intermediate. Each surface of the cell is defined as a single self-contact surface (i.e., the LS-DYNA * CONTACT_AUTOMATIC_SINGLE_SURFACE). Besides, the surface-to-surface contact (i.e., the LS-DYNA * CONTACT_AUTOMATIC_SURFACE_TO_SURFACE) was used between the specimen and two rigid plates. Meshing of two models was done using SR4 elements, and the mesh method was swept with quad-dominated elements, as shown in Fig. 6. The material properties selected to run the simulation are listed in Table 2.

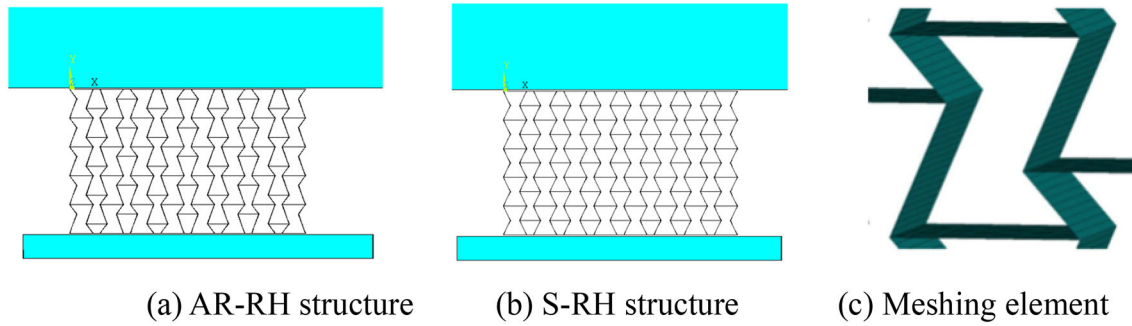


Fig. 6. Simulation model

Table 2. Material parameters of simulation

Materials	Elastic modulus (GPa)	Density (kg/m ³)	Poisson's ratio (μ)	Shear modulus (GPa)	Yield stress σ_s (MPa)
Rigid slab	210	7800	0.3	—	—
Honeycomb model	161	7625	0.29	1	402

5. Results of Test and Simulation

5.1. Evaluation Index of Structural Energy Absorption

The nominal stress σ and nominal strain ε of the in-plane impact test based on the novel AR-RH structure with negative Poisson's ratio are defined as follows:

$$\sigma = \frac{F}{A} \quad (1)$$

$$\varepsilon = \frac{\delta}{h} \quad (2)$$

where F is the compression reaction of the drop hammer, $A = lz_l$ is the cross-sectional area of the test specimen, δ is the compression displacement, and h is the length of the model in vertical. The platform stress and the specific energy absorption (E_{SEA}) are two important indices to evaluate the energy absorption capacity of porous structures [24, 28]. The platform stress of the porous structure can be averaged from the stress values of the platform stage in the stress-strain curve, which can be expressed as:

$$\sigma_p = \frac{1}{\varepsilon_d - \varepsilon_{cr}} \int_{\varepsilon_{cr}}^{\varepsilon_d} \sigma(\varepsilon) d\varepsilon \quad (3)$$

where $\sigma(\varepsilon)$ is the nominal stress with the change of strain, ε_{cr} is the nominal strain corresponding to the peak value of initial stress (the value of ε_{cr} is relatively small, and $\varepsilon_{cr} = 0.02$ in this paper), and ε_d is the maximum strain value before the material is compressed and compacted. To avoid the influence of human selection factors, the energy absorption efficiency method [29] was used to determine the dense strain, which is:

$$\left. \frac{d\beta(\varepsilon)}{d\varepsilon} \right|_{\varepsilon=\varepsilon_d} = 0 \quad (4)$$

where $\beta(\varepsilon)$ represents the energy absorption efficiency parameter and is defined as the ratio of the energy absorbed under the given nominal strain to the corresponding nominal stress:

$$\beta(\varepsilon) = \frac{\int_0^{\varepsilon} \sigma(\varepsilon) d\varepsilon}{\sigma(\varepsilon)} \quad (5)$$

The nominal stress-strain curve and energy absorption efficiency curve of the structure are shown in Fig. 7. There are many local maximum values in the energy efficiency curve of porous structure. In this study, the final maximum point (i.e., the point where the energy absorption efficiency curve begins to

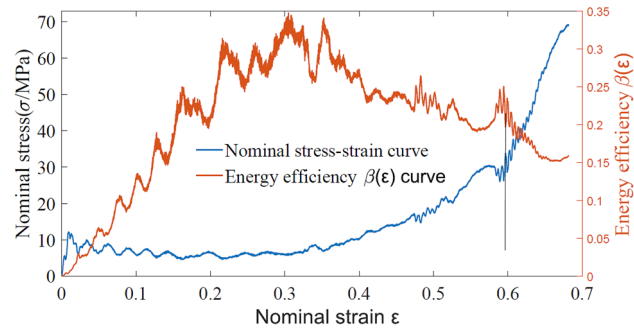


Fig. 7. Nominal stress–strain curve and energy absorption efficiency curve of honeycomb structure

decline rapidly) was defined, and the corresponding nominal strain was used as the compaction point, which is the compaction strain value, as shown in the auxiliary line in Fig. 8.

The other factor, the specific energy absorption, E_{SEA} , is defined as:

$$E_{SEA} = \frac{\int_0^{\varepsilon} \sigma(\varepsilon) d\varepsilon}{M} \quad (6)$$

where M indicates the mass of the structure, and the larger is the specific energy absorption, the better is the energy absorption effect of the structure.

5.2. Results of Test and Simulation

5.2.1. Dynamic Response Analysis

The typical impacting stress–strain curves for both models are shown in Fig. 8, and the effective stress contours of AR-RH and S-RH structures are displayed in Fig. 9. The finite element simulation results of two structures are fairly consistent with the experimental ones, showing the reliability of the numerical simulation.

By comparing the two structures, it can be seen that both structures exhibit negative Poisson's ratio and elastic–plastic collapse. There was no significant difference in Young's moduli of the AR-RH and S-RH structures. The compressive strength of S-RH structure was higher than that of the AR-RH structure, but the AR-RH structure has higher platform stress. Junction rotation can absorb energy [30, 31]. Here, the AR-RH structure can rotate more after buckling than the S-RH structure, so the energy absorption of AR-RH structure is greater than the S-RH structure. Furthermore, Fig. 9 shows that the stiffness of the AR-RH structure is higher than that of the S-RH structure.

Figure 8a–c presents comparisons of nominal stress–strain curves at three impact velocities ($V = 3$ m/s, $V = 4$ m/s and $V = 5$ m/s). There are three stages: elastic stage, plateau stage and dense stage. The compression stress and dense strain increase along with the increase in the impact velocity. No obvious change can be observed in the elastic stage or the plateau stage, but the dense strain obviously increases with the impact velocity.

The specific energy absorption is equal to the total energy absorption by the total mass, as seen in Eq. (6). There is a close link between the platform stress and energy absorption: The higher the platform stress, the better is the energy absorption. In Fig. 10, when the strain is below 0.1, the two structures have similar energy absorptions and Young's moduli; but when the strain is between 0.1 and 0.4, the AR-RH structure shows better energy absorption compared with the normal S-RH structure. This is because when the strain is less than 0.1, the structure behaves elastic deformation, and with same thickness, the whole stiffness of the AR-RH structure is similar to that of the S-RH structure. As the strain increases, the local cells of the S-RH structure firstly become buckled and the collapse stresses develop, but the cells of the AR-RH structure can prevent from buckling due to the asymmetry and rotatability, producing a more stable platform stress. For example, when the strain is 0.3 at the same impact velocity, the energy absorption of the AR-RH structure is about 1.32 times of the S-RH structure.

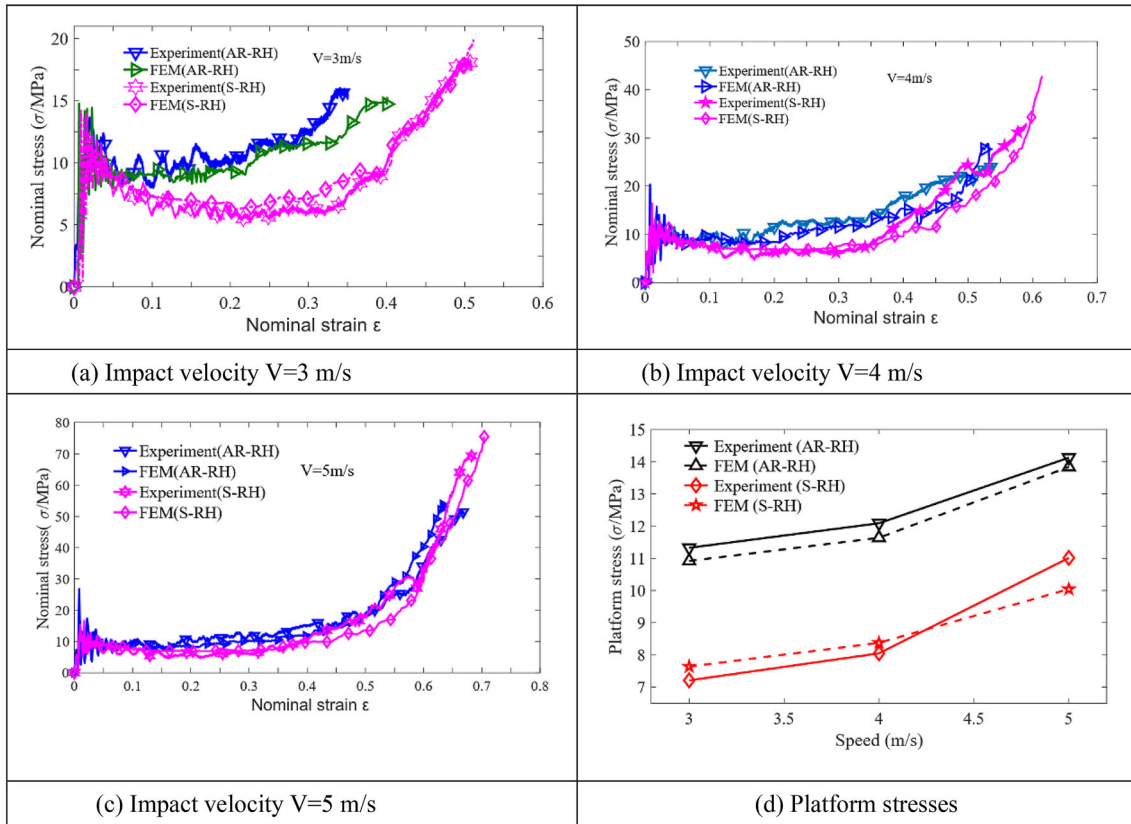


Fig. 8. Dynamic response curves and platform stresses at different impact velocities

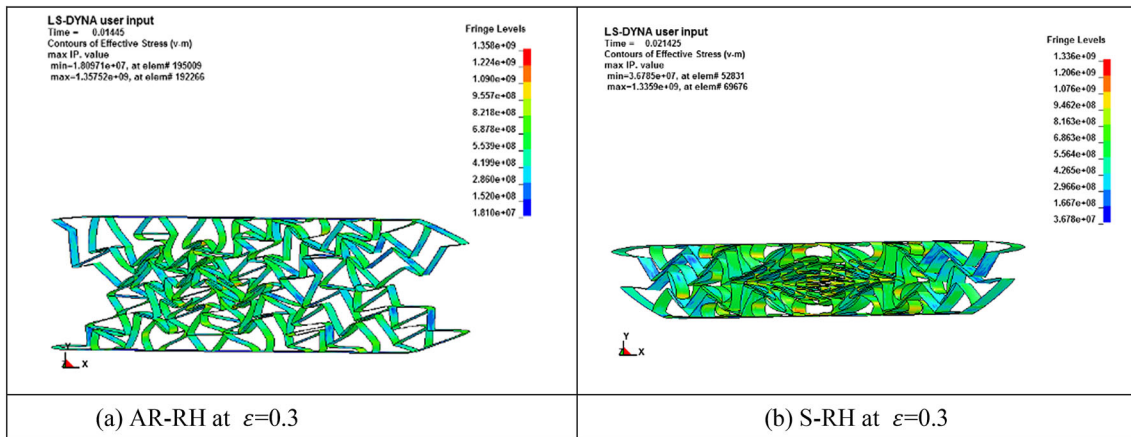


Fig. 9. Contours of effective stress of AR-RH and S-RH structures

5.2.2. Failure Mode Analysis

Figure 11 shows the deformation patterns of six specimens at different impact velocities (i.e., 3 m/s, 4 m/s and 5 m/s). Overall, the deformation trends of the six specimens are similar. After being subjected to the impact load, the compression deformation appears in the vertical direction, while the concave deformations at two free edges appear in the horizontal direction, and this is obviously due to the effect of negative Poisson's ratio. The AR-RH structure has less deformation because of its greater stiffness than the S-RH structure. When the impact velocity is 3 m/s, the deformation patterns of AR-RH and S-RH are very similar, and the shear band is formed on the diagonal line, leading to the

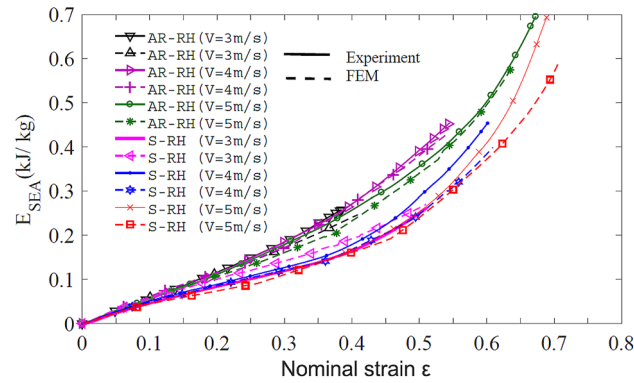


Fig. 10. Specific energy absorption curves of AR-RH and S-RH structures

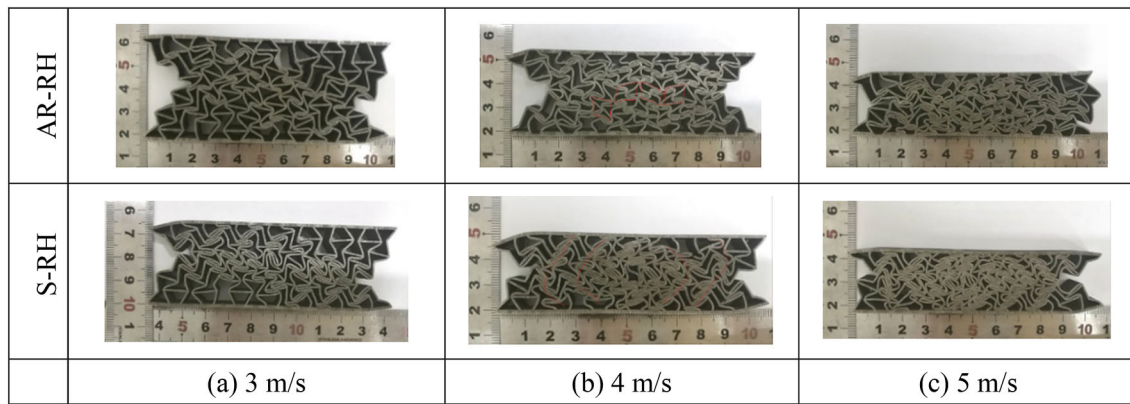


Fig. 11. Detailed deformation and failure modes of each structure

shear deformation of the cell unit on the diagonal in the upper left and lower right corners, and obvious warping occurs in the upper left and lower right corners.

When the velocity is higher than 4 m/s, the deformation mechanisms of the two models are different. It is mainly the internal concave mechanism. For a single cell unit, when the cell unit is squeezed, the two free sides will be depressed toward the center. When the whole cell unit is collapsed, the cell walls on both sides of the cell have some degree of plastic deformation, and the upper and lower cell walls are only superimposed together to form a dense band and its compaction band shapes are similar to the parentheses, “()”, appearing on both sides, which can be observed from Fig. 11. Furthermore, the compaction zones of the S-RH structure also present the parenthesis type, “()”, on both sides near the free boundaries with higher impact velocity.

However, the deformation of cell unit in the AR-RH structure shows another form. When the cell unit is compressed and deforms, the whole cell unit rotates by a certain angle, while the cell walls on both sides of the cell unit are compressed, so the deformation of the cell structure and the lower parenchyma is changed, rather than simply being superimposed together. However, with the deformation of the side walls, the plastic deformation of the upper and lower walls of the cell unit occurs in different degrees. The deformation of the AR-RH structure is mainly based on the deformation mode of the “I” type.

5.3. The Effect of Asymmetry on Energy Absorption

On the basis of previous study, this section studies the influence of cell asymmetry on structural energy absorption. There are four modes with different concave heights, as shown in Fig. 12: $m_1 = \frac{3}{12}h, m_2 = \frac{4}{12}h, m_3 = \frac{5}{12}h, m_4 = \frac{6}{12}h$.

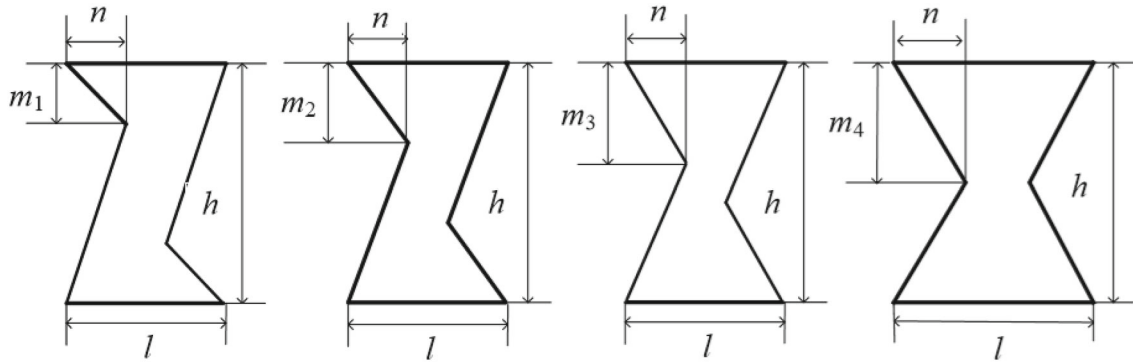


Fig. 12. Four modes with different forms of asymmetry

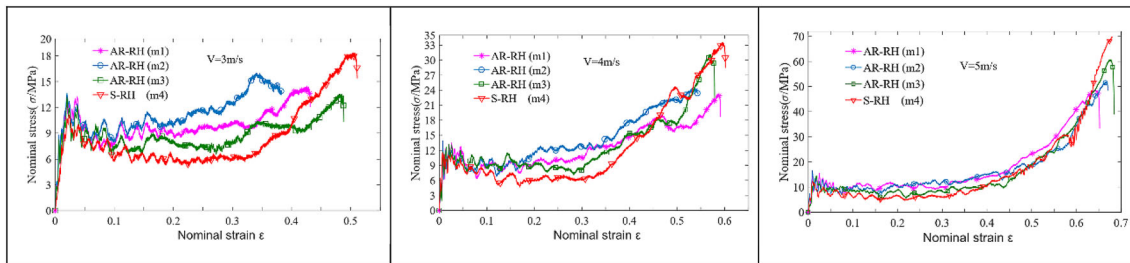


Fig. 13. Stress-strain curves of four modes at the impact velocities of 3 m/s, 4 m/s and 5 m/s, respectively

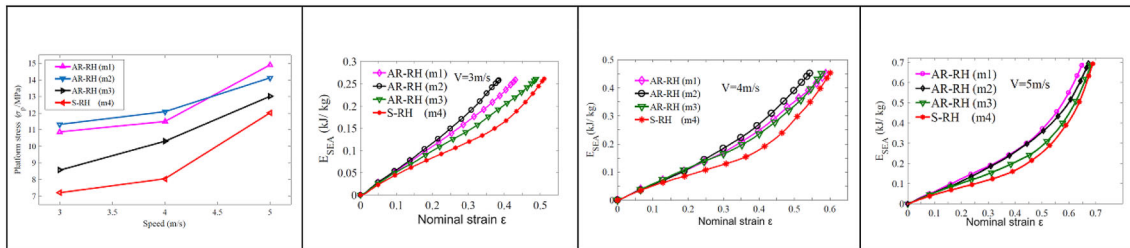


Fig. 14. Energy curves of four modes at different impact velocities

In general, with the decrease in concave height, the rotatable performance is gradually improved, and the platform stress of the structure is gradually increased; meanwhile, the energy absorption capacity and platform stress are both significantly improved. Here, the contribution of rotation performance to energy absorption is fully demonstrated in Figs. 13 and 14a. However, it is found that the concave height cannot be too small, because a very small concave height of cell will cause the length of the inclined rod to increase, leading to easier buckling of the inclined rod, and reductions of the platform stress and energy absorption capacity. Therefore, there is an optimal value of the concave height with best energy absorption capacity. In this study, when $m_2 = \frac{4}{12}h$, it has the better energy absorption capacity than others.

The simulation results of stress-strain curves and energy curve are provided in Figs. 13 and 14 for different concave heights at different impact velocities, i.e., 3 m/s, 4 m/s and 5 m/s. It is worth pointing out that the energy absorption is better with stronger asymmetry due to the greater platform stress at the plateau stage, especially at 3 m/s and 4 m/s. When the velocity is 5 m/s, the effect of asymmetry on energy absorption capacity is gradually weakened.

Above all, the sensitivity effect of asymmetry on the energy absorption behavior needs to be considered when designing a honeycomb structure.

6. Conclusion

A new asymmetric and rotatable re-entrant honeycomb (AR-RH) structure with better energy absorption and buffering characteristics than the normal symmetric and re-entrant honeycomb (S-RH) structure has been proposed. The novel AR-RH structure and normal S-RH structure have been realized by 3D printing technology. The in-plane impact dynamics of the two structural models were studied by means of drop hammer impact test and finite element simulation. The results show that the AR-RH structure has better energy absorption effect and higher plateau stress than the traditional S-RH structure. More importantly, it has been verified that the rotatable mechanism of cell can indeed absorb additional energy. The analysis of asymmetry demonstrated that an increase in concave height of structure could enhance the ability of energy absorption. The proposed asymmetric and rotatable re-entrant honeycomb structure is a promising one for protective applications against blast loading. Further numerical designs and experiments are under preparation to validate the concept.

Acknowledgements. This work is supported by the State Key for Strength and Vibration of Mechanical Structures of Xi'an Jiaotong University (No. SV2018-KF-32) and the Natural Science Foundation of Guangdong Province of China (2020A1515011064).

Compliance with ethical standards

Data availability statement All data, models and code generated or used during the study appear in the submitted article.

References

- [1] Fu M-H, Chen Y, Hu L-L. A novel auxetic honeycomb with enhanced in-plane stiffness and buckling strength. *Compos Struct.* 2017;160:574–85.
- [2] Zhang X, Ding H, An L, Wang X. Numerical investigation on dynamic crushing behavior of auxetic honeycombs with various cell-wall angles. *Adv Mech Eng.* 2015;7(2):679678.
- [3] Huang J, Zhang Q, Scarpa F, Liu Y, Leng J. In-plane elasticity of a novel auxetic honeycomb design. *Compos B Eng.* 2017;110:72–82.
- [4] Imbalzano G, Tran P, Ngo TD, Lee PV. A numerical study of auxetic composite panels under blast loadings. *Compos Struct.* 2016;135:339–52.
- [5] Boldrin L, Hummel S, Scarpa F, Di Maio D, Lira C, Ruzzene M, et al. Dynamic behaviour of auxetic gradient composite hexagonal honeycombs. *Compos Struct.* 2016;149:114–24.
- [6] Liu Y, Hu H. A review on auxetic structures and polymeric materials. *Sci Res Essays.* 2010;5(10):1052–63.
- [7] Yang W, Li Z-M, Shi W, Xie B-H, Yang M-B. Review on auxetic materials. *J Mater Sci.* 2004;39(10):3269–79.
- [8] Evans KE. Auxetic polymers: a new range of materials. *Endeavour.* 1991;15(4):170–4.
- [9] Thill C, Etches J, Bond I, Potter K, Weaver P. Morphing skins. *Aeronaut J.* 2008;112(1129):117–39.
- [10] Martin J, Heyder-Bruckner JJ, Remillat C, Scarpa F, Potter K, Ruzzene M. The hexachiral prismatic wingbox concept. *Physica Status Solidi (b).* 2008;245(3):570–7.
- [11] Masters I, Evans K. Models for the elastic deformation of honeycombs. *Compos Struct.* 1996;35(4):403–22.
- [12] Spadoni A, Ruzzene M, Scarpa F. Dynamic response of chiral truss-core assemblies. *J Intell Mater Syst Struct.* 2006;17(11):941–52.
- [13] Hassan M, Scarpa F, Ruzzene M, Mohammed N. Smart shape memory alloy chiral honeycomb. *Mater Sci Eng A.* 2008;481:654–7.
- [14] Bornengo D, Scarpa F, Remillat C. Evaluation of hexagonal chiral structure for morphing airfoil concept. *Proc Inst Mech Eng Part G J Aerosp Eng.* 2005;219(3):185–92.
- [15] Scarpa F, Burriesci G, Smith F, Chambers B. Mechanical and electromagnetic behaviour of auxetic honeycomb structures. *Aeronaut J.* 2003;107(1069):175.
- [16] Frost HJ, Ashby MF. *Deformation mechanism maps: the plasticity and creep of metals and ceramics.* Oxford: Pergamon Press; 1982.
- [17] Choi J, Lakes R. Analysis of elastic modulus of conventional foams and of re-entrant foam materials with a negative Poisson's ratio. *Int J Mech Sci.* 1995;37(1):51–9.
- [18] Zhang Z, Hu H, Xu B. An elastic analysis of a honeycomb structure with negative Poisson's ratio. *Smart Mater Struct.* 2013;22(8):084006.
- [19] Zied K, Osman M, Elmahdy T. Enhancement of the in-plane stiffness of the hexagonal re-entrant auxetic honeycomb cores. *Physica Status Solidi (b).* 2015;252(12):2685–92.

- [20] Zhang X-C, Liu Y, Li N. In-plane dynamic crushing of honeycombs with negative Poisson's ratio effects. *Explos Shock Waves*. 2012;32(5):475–82.
- [21] Hou X, Deng Z, Zhang K. Dynamic crushing strength analysis of auxetic honeycombs. *Acta Mech Solida Sin*. 2016;29(5):490–501.
- [22] Lu Z, Zhao Y. A two-dimensional multi-cell material mechanics model with negative Poisson's ratio effect. *J Beijing Univ Aeronaut Astronaut*. 2006;32(05):594–7.
- [23] Shi Q. Performance characterization and optimum design of negative Poisson ratio honeycomb core. Doctoral dissertation, Harbin Institute of Technology, 2014.
- [24] Fan X, Yin X, Tao Y. Mechanical behavior and energy absorption of graded honeycomb materials under out-of-plane dynamic compression. *Guti Lixue Xuebao/Acta Mech Sol Sin*. 2015;36:114–22.
- [25] Panda B, Leite M, Biswal BB, Niu X, Garg A. Experimental and numerical modelling of mechanical properties of 3D printed honeycomb structures. *Measurement*. 2018;116:495–506.
- [26] Wang Z. Recent advances in novel metallic honeycomb structure. *Compos B Eng*. 2019;166:731–41.
- [27] Testing ASf, Materials, editors. D638-08: Standard Test Method for Tensile Properties of Plastics;2008. ASTM.
- [28] Gibson LJ, Ashby MF. *Cellular solids: structure and properties*. Cambridge: Cambridge University Press; 1999.
- [29] Tan PJ, Reid SR, Harrigan JJ, Zou Z, Li S. Dynamic compressive strength properties of aluminium foams. Part I—experimental data and observations. *J Mech Phys Solids*. 2005;53(10):2174–205.
- [30] Zhu H, Thorpe S, Windle A. The effect of cell irregularity on the high strain compression of 2D Voronoi honeycombs. *Int J Solids Struct*. 2006;43(5):1061–78.
- [31] Zhu HX, Mills N. The in-plane non-linear compression of regular honeycombs. *Int J Solids Struct*. 2000;37(13):1931–49.